

# Trap States, Electric Fields, and Phase Segregation in Mixed-Halide Perovskite Photovoltaic Devices

Alexander J. Knight, Jay B. Patel, Henry J. Snaith, Michael B. Johnston, and Laura M. Herz\*

Mixed-halide perovskites are essential for use in all-perovskite or perovskite–silicon tandem solar cells due to their tunable bandgap. However, trap states and halide segregation currently present the two main challenges for efficient mixed-halide perovskite technologies. Here photoluminescence techniques are used to study trap states and halide segregation in full mixed-halide perovskite photovoltaic devices. This work identifies three distinct defect species in the perovskite material: a charged, mobile defect that traps charge-carriers in the perovskite, a charge-neutral defect that induces halide segregation, and a charged, mobile defect that screens the perovskite from external electric fields. These three defects are proposed to be MA<sup>+</sup> interstitials, crystal distortions, and halide vacancies and/or interstitials, respectively. Finally, external quantum efficiency measurements show that photoexcited charge-carriers can be extracted from the iodide-rich low-bandgap regions of the phase-segregated perovskite formed under illumination, suggesting the existence of charge-carrier percolation pathways through grain boundaries where phase-segregation may occur.

mixture thereof) allows for tuning and control over the bandgap of the resulting material across the approximate range 1.5–2.3 eV.<sup>[11–14]</sup> The flexible bandgap of mixed iodide/bromide perovskites have made them indispensable so far in the creation of highly efficient perovskite–silicon and perovskite–perovskite tandem solar cells.<sup>[3–7]</sup> However, photoluminescence (PL) and X-ray diffraction (XRD) techniques have shown that upon illumination the halide ions within some mixed-halide perovskites demix to form regions of differing composition—and differing bandgap—within the same perovskite film.<sup>[15,16]</sup> The spontaneous halide segregation and formation of a spatially inhomogeneous bandgap diminishes the charge-carrier transport properties of the perovskite film and undermines the value

## 1. Introduction

Over the last few years metal halide perovskites (MHPs) have cemented their reputation as efficient, versatile, and easy to manufacture light energy harvesters and are now arguably the leading candidate for the next generation of solar cells.<sup>[1,2]</sup> The recent developments in perovskite–silicon<sup>[3,4]</sup> and perovskite–perovskite<sup>[5–8]</sup> tandem solar cells have further demonstrated the light-harvesting capability of perovskite technology and present a promising future avenue for MHPs commercially. A critical aspect of forming practical tandem solar cells is selecting materials with complementary bandgaps, since this allows for more efficient energy extraction from the solar spectrum than theoretically allowed for a single-junction solar cell.<sup>[9,10]</sup> It has been demonstrated that mixing iodide and bromide ions onto the anion sites in lead-based perovskites (stoichiometric formula APb(Br<sub>x</sub>I<sub>1–x</sub>)<sub>3</sub>, where A is typically MA<sup>+</sup>, FA<sup>+</sup>, Cs<sup>+</sup>, or a

of a selectable bandgap, dramatically reducing the viability of these materials for use as part of a tandem solar device.<sup>[17–19]</sup> Interestingly, once the perovskite film is removed from the illumination source, the segregated halide ions remix over the course of tens of minutes to hours, and the film returns to its initial state.<sup>[15]</sup> While it has been shown that improving the crystallinity of the perovskite can reduce the influence of halide segregation<sup>[20–22]</sup> and that photoexcited charge-carriers seem to drive the underlying mechanism,<sup>[17,19]</sup> there are still many important open questions as to the fundamental processes behind halide segregation.

In a recent study we found that electronic trap states and trapped charge-carriers play an important part of the underlying halide segregation mechanism.<sup>[23]</sup> By varying the intensity of illumination upon a mixed-halide perovskite film and controlling for the total number of cumulative incident photons, we were able to show that the fraction of charge-carriers that recombined through trap states was correlated with the amount of halide segregation observed. Additionally, electronic trap states are responsible for the majority of the preventable losses in solar cell performance under typical working conditions, and so understanding and passivating trap states represents one of the greatest challenges for mixed-halide perovskites. A particular consideration is also that a multitude of different point defects may exist in metal halide perovskites, which may have different mobilities, charges, spatial distributions, and effects on optoelectronic properties. A vast amount of research has been performed on the nature of defects and trap states

A. J. Knight, Dr. J. B. Patel, Prof. H. J. Snaith, Prof. M. B. Johnston, Prof. L. M. Herz  
Department of Physics  
University of Oxford  
Clarendon Laboratory  
Parks Road, Oxford OX1 3PU, UK  
E-mail: laura.herz@physics.ox.ac.uk

 The ORCID identification number(s) for the author(s) of this article can be found under <https://doi.org/10.1002/aenm.201903488>.

DOI: 10.1002/aenm.201903488

in metal halide perovskites,<sup>[24,25]</sup> but despite this large body of research many unknowns remain, such as the role of defects at grain boundaries, and how trap states relate to ion migration.<sup>[25]</sup>

Halide segregation and electronic trap states represent two of the most substantial obstacles for the incorporation of mixed-halide perovskite into stable and efficient tandem solar cells. Particularly important for photovoltaic devices is the interaction of halide ions and trap states with electric fields, since efficient power extraction depends on the combination of external and built-in electric fields within a solar device. Additionally, it has been observed that electric fields can influence the PL from MAPbI<sub>3</sub> films through trap state movement,<sup>[26–29]</sup> a process which—similarly to halide segregation—is attributed to the movement of mobile, charged species in the perovskite material. Therefore, in order to fully understand the limiting aspects of mixed-halide perovskite devices under normal working conditions it is necessary to consider the complex interaction between electric fields, different electronic trap states and halide segregation. In this study we performed PL, time correlated single photon counting (TCSPC), and external quantum efficiency (EQE) measurements on full MAPb(Br<sub>0.5</sub>I<sub>0.5</sub>)<sub>3</sub> photovoltaic device stacks under an external bias in order to gain a greater understanding of the underlying processes and charge-carrier pathways in segregating mixed-halide perovskite materials. We note that while even state-of-the-art MAPb(Br<sub>0.5</sub>I<sub>0.5</sub>)<sub>3</sub> perovskite photovoltaic devices are relatively inefficient compared to those composed of other mixed-halide perovskites,<sup>[11,13,30,31]</sup> MAPb(Br<sub>0.5</sub>I<sub>0.5</sub>)<sub>3</sub> still represents an ideal material for studies on halide segregation because it segregates quickly under ≈1 sun illumination intensities, allowing repeated measurements to be made in a reasonable time frame.<sup>[15]</sup> We find evidence for three species of defects in the perovskite material: First, a charged, mobile trap species, proposed to be MA<sup>+</sup> interstitial defects in the perovskite crystal, is observed to detrimentally affect the radiative efficiency of the perovskite material. Second, following our previous work,<sup>[23]</sup> we suggest that charge neutral crystal distortions in the perovskite structure trap photoexcited charge-carriers and contribute to the halide segregation mechanism. Third, charged, mobile defects, proposed to be halide vacancies and/or interstitials in the perovskite material, are observed to rapidly screen the perovskite layer in our devices upon a change in the applied external bias. Additionally, we find that while halide segregation is detrimental for current extraction from a mixed-halide perovskite solar cell, some current is still extracted from the forming iodide-rich perovskite domains of such a solar cell under illumination. The extraction of current from the low-bandgap domains suggests the existence of percolation pathways between the iodide-rich regions of the perovskite and the charge transport layers in the device stack, which we postulate to be formed at the grain boundaries in the perovskite layer. Finally, we summarize our understanding gained from this study of the charge-carrier pathways in mixed-halide perovskite devices through a Sankey (flow) diagram.

## 2. Defect Species in MAPb(Br<sub>0.5</sub>I<sub>0.5</sub>)<sub>3</sub>

PL and TCSPC measurements are sensitive to both the charge-carrier population in a material and the rules for radiative and nonradiative decay, and so they are powerful tools in

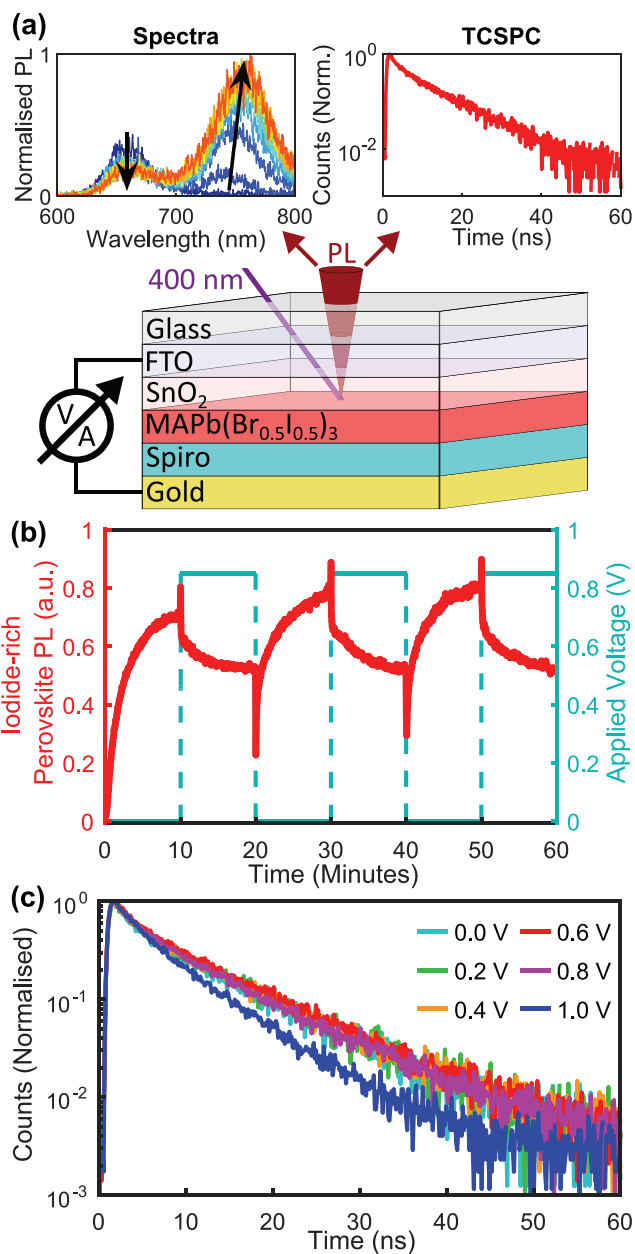


**Figure 1.** Experimental overview and results from PL measurements of a MAPb(Br<sub>0.5</sub>I<sub>0.5</sub>)<sub>3</sub> device held at various applied voltages. a) Device stack and experimental schematic for PL measurements. Example PL and TCSPC data taken under the same experimental conditions as (b) and (c), respectively, are also shown. b) The behavior of the low-energy PL (PL spectra integrated from 720 to 770 nm and plotted in red) as a changing voltage (plotted in blue) is applied across a mixed-halide perovskite device under 400 nm, 110 mW cm<sup>-2</sup>, continuous wave illumination. c) TCSPC decay traces measured at the low-energy PL peak (750 nm) of a mixed-halide perovskite device under various applied voltages and under 400 nm, 1400 mW cm<sup>-2</sup>, 5 MHz pulsed laser illumination. The device was held at each target voltage for at least 1 h before each 120 s TCSPC measurement was taken, and the applied voltages were applied in descending order.

uncovering the charge-carrier pathways in mixed-halide perovskites. **Figure 1a** shows a schematic of the basic experimental setup and device layers for our study, alongside a set of example

PL spectra and a TCSPC trace. Basic characterization results for our perovskite material and devices—including absorbance spectrum (Figure S1, Supporting Information), XRD pattern (Figure S2, Supporting Information), cross-sectional scanning electron microscopy image (Figure S3, Supporting Information), current–voltage scans (Figure S4, Supporting Information), and stabilized power output graph (Figure S4 inset, Supporting Information)—are reported in Section S2 of the Supporting Information. As shown in the example PL spectra in Figure 1a, upon illumination of our device, the PL peak attributed to the mixed-halide perovskite phase (emission around 665 nm) diminished, and a lower energy peak (around 745 nm) was observed to emerge. These changes in the PL spectrum have been well-established by the literature to result from photoexcited charge-carriers funneling from the well-mixed perovskite phase into the lower-bandgap regions of iodide-rich perovskite that form under illumination as halide segregation takes place.<sup>[15,32]</sup> Our mixed-halide device stack was built upon a glass substrate, with SnO<sub>2</sub> and 2,2',7,7'-Tetrakis[*N,N*-di(4-methoxyphenyl)amino]-9,9'-spirobifluorene (spiro-OMeTAD) used as the electron and hole transport layers, respectively. Gold and fluorine doped tin oxide (FTO) were used as the top and bottom contact layers, respectively. Applying a voltage between the contact layers allowed us to examine the influence of an electric field on the charge-carrier dynamics within the perovskite layer.

### 2.1. Influence of Charged, Mobile Trap States

Figure 1b shows the PL intensity emitted around 745 nm from a fresh MAPb(Br<sub>0.5</sub>I<sub>0.5</sub>)<sub>3</sub> photovoltaic device as an applied voltage across the device is changed multiple times between 0 V (short circuit) and 0.85 V. In order to induce halide segregation and to cause the emission of PL, our device stack was illuminated with a continuous wave, 400 nm laser at 110 mW cm<sup>-2</sup> intensity, similar to 1 sun intensity. Spectral measurements were made every 3 s, and in order to better follow the growth of the iodide-rich regions in the perovskite layer, the corresponding low-energy peak in the PL spectrum was integrated (from 720 to 770 nm) and is plotted in red in Figure 1b as a PL intensity. The voltage applied across the device is plotted in cyan in Figure 1b, with 0 V being first held across the device for 10 min as the perovskite layer initially segregated, and subsequent 10 min periods of applied voltage alternating between 0.85 and 0 V. It is important to note that in *n-i-p* photovoltaic devices such as ours, a built-in electric field is generated between the *n* and *p* layers, and this field permanently exists across the perovskite layer. The external voltage that we applied across the contact layers counteracted this built-in field, allowing control over the total field across the perovskite layer. For example, at 0 V applied bias (i.e., at short circuit) there was no counter-field working against the built-in field and so the voltage across the perovskite layer was relatively high. At an applied bias of 0.85 V the built-in field was mostly cancelled out by the applied field, resulting in a much lower net field across the perovskite layer (as shown by current extraction measurements plotted in Figure S5 of the Supporting Information, 0.85 V was close to the open circuit voltage of our device, the *V*<sub>OC</sub>). As shown in our previous study,<sup>[23]</sup> the combination of

a thick encapsulation layer (here a role provided by the spiro-OMeTAD and gold layers) and holding the perovskite device under vacuum (at a pressure of  $\approx 10^{-1}$  mbar for this experiment) prevents any significant interaction between the perovskite and the surrounding atmosphere. As a result of this protection, we note that we observed no long-term trends attributable to atmospheric influence<sup>[33,34]</sup> in data presented either in Figure 1 or the rest of this study.

During the first 10 min under illumination at 0 V applied bias, Figure 1b shows a clear rise and plateau of the iodide-rich perovskite PL, which is ascribed to the growth and stabilization of the iodide-rich domains within the perovskite layer.<sup>[15]</sup> Thereafter, whenever the applied voltage was increased from 0 to 0.85 V the PL intensity initially spiked sharply upward, before slowly decaying to a lower value. Conversely, when the applied voltage was decreased from 0.85 to 0 V the PL intensity initially spiked sharply downward before slowly rising to a higher value. The sharp spikes follow the behavior expected of a typical solar cell (see Figure S6 in the Supporting Information for an example of the PL emitted from a solution processed MAPbI<sub>3</sub> device), as at an applied bias of 0 V (0.85 V), the extracted current was maximal (minimal), and so fewer (more) charge-carriers were available to recombine radiatively, leading to less (more) PL. The extracted current from the measured MAPb(Br<sub>0.5</sub>I<sub>0.5</sub>)<sub>3</sub> device can be found in Figure S5 in the Supporting Information and was indeed higher and lower at 0 and 0.85 V applied bias, respectively. We therefore conclude that the spikes in the PL intensity observed in Figure 1b were the result of a higher or lower charge-carrier density within the perovskite layer depending on the level of current extraction present at the applied voltage.

The slower changes in PL intensity following the initial spike at the start of each 10 min period (Figure 1b) suggests that the radiative efficiency of the perovskite layer slowly increased or decreased when held under 0 or 0.85 V applied bias, respectively. These slow changes did not coincide with any significant change in the illumination source (which was held constant), and the extracted current is shown in Figure S5 (Supporting Information) to have reached equilibrium much faster than the PL upon each applied voltage change, ruling out these two alternative explanations. In order for the radiative efficiency to change, we conclude that nonradiative recombination pathways (i.e., trap states) increasingly interacted with the photoexcited charge-carrier population as the applied voltage across the device was increased, reducing the emitted PL. We note that we did not find such behavior under similar conditions for a solution processed MAPbI<sub>3</sub> device (see Figure S6 in the Supporting Information), likely due to intrinsic material differences affording different amounts of ion migration between the two materials, and differences in device performance altering how much charge-carrier extraction affected the emitted PL. Correlations between applied voltage and loss of radiative efficiency have previously been reported in MAPbI<sub>3</sub> and other metal halide perovskites.<sup>[26–29,35]</sup>

To further study the influence of electric field on the rate of trap mediated recombination, we performed time-resolved PL measurements on a perovskite photovoltaic device at various voltages, with the results presented in Figure 1c. Before each measurement, the same device was subjected to 1 h of

illumination with the target voltage applied across the device in order to ensure that any mobile ions within the perovskite layer had reached equilibrium. An additional period of 0.5 h under illumination and bias was applied at the start of the experiment to account for the fact that the mobile ions (particularly the segregating halide ions) would need more time to reach equilibrium when the illumination and bias was applied to the initially fresh device. The illumination source was a 400 nm laser pulsed at 5 MHz and at  $1400 \text{ mW cm}^{-2}$  intensity, the accumulation time for each trace was 120 s and the measured PL wavelength was at 750 nm, near the center of the iodide-rich perovskite PL peak.

Figure 1c shows that the charge-carrier recombination rate within the iodide-rich regions of the perovskite layer was roughly constant at applied voltages lower than  $\approx 0.8 \text{ V}$ , and higher at  $\approx 1.0 \text{ V}$  applied bias. We note that in order to ensure that the change in charge-carrier lifetimes was not the result of material degradation over the course of several hours, the set voltages were applied in decreasing value, i.e., with  $1.0 \text{ V}$  applied first. In Figure S7 (Supporting Information) we present near-identical data from a similar experiment in which the set voltages were applied in ascending order, further showing that the changes to the charge-carrier lifetimes were caused by the resulting bias across the perovskite, not material degradation over the course of the experiment. The increase in charge-carrier recombination rate at high applied voltage could be a consequence of an increase in trap-mediated recombination, radiative recombination, current extraction, or a combination of these factors (Auger recombination is assumed to be negligible at the  $1400 \text{ mW cm}^{-2}$  illumination intensity used after at most a few nanoseconds into the decay dynamics<sup>[36]</sup>). We later show that the iodide-rich regions in the segregated perovskite layer do contribute to the current extracted from the mixed-halide perovskite device, however an increase in applied voltage serves to decrease the extracted current, which lengthens the charge-carrier lifetimes (this behavior is highlighted in Figure S8 in the Supporting Information for a  $\text{MAPbI}_3$  device). Additionally, it was shown in Figure 1b that the rate of radiative recombination (which produces PL) does not increase at high applied voltages, allowing us to conclude that the shortening of charge-carrier lifetimes at an applied bias of  $1.0 \text{ V}$  was primarily due to an increase in the rate of trap-mediated recombination in the perovskite layer at high applied voltage. Thus, Figure 1c corroborates the evidence in Figure 1b that a higher applied voltage increases the rate of trap-mediated charge-carrier recombination in  $\text{MAPb}(\text{Br}_{0.5}\text{I}_{0.5})_3$  photovoltaic devices. We note that with our setup, changes to the radiative efficiency of our devices were more easily resolved through PL measurements than with TCSPC measurements (as also evident from PL and TCSPC measurements of a  $\text{MAPbI}_3$  device—see Figures S6 and S8, respectively).

The timescale and nature of the changes that occur in the PL presented in Figure 1b are similar to those that have been observed to occur in the single-halide perovskite  $\text{MAPbI}_3$  under similar bias conditions.<sup>[26–29]</sup> Therefore, as has been done in the literature for  $\text{MAPbI}_3$ , we attribute the decrease in PL intensity (Figure 1b) and charge-carrier lifetime (Figure 1c) that occurs with an increased applied voltage to the movement of charged, mobile trap states in the perovskite. Figure 1 shows that the radiative efficiency of the perovskite layer is highest at  $0 \text{ V}$

applied bias, when the total electric field across the perovskite results solely from the built-in field, suggesting that the mobile trap states are forced away from the illumination side of the device—where the density of photoexcited charge-carriers is highest—by the built-in potential field generated by the extraction layers. In n-i-p devices, such as ours here, the illuminated volume of the perovskite layer—where the charge-carriers are photogenerated—is near the positively charged, electron extraction layer, which suggests that the mobile trap states carry a positive charge and accumulate near the hole extraction layer at  $0 \text{ V}$  applied bias. Due to their charge, these proposed trap states will attract and trap electrons, but repel and be largely benign to holes. The quenching of the PL intensity and lifetime is then explained as follows: at  $0 \text{ V}$  applied bias, a large voltage is generated across the perovskite layer by the built-in field. This potential forces the positive trap states toward the spiro-OMeTAD side of the device, and collects the electrons into the  $\text{SnO}_2$  layer, away from the trap states. Thus at low applied voltage the trap states and the electrons are separated, leading to a limited amount of trap-mediated recombination, and therefore a higher rate of radiative recombination despite the significant current extraction. At an applied bias of  $0.85 \text{ V}$ , the applied electric field significantly offsets the built-in electric field, and so the migratory trap states are less appreciably accumulated at the spiro-OMeTAD side of the device and instead diffuse more evenly throughout the perovskite layer, allowing them to interact with and trap the photogenerated electrons. The larger overlap of trap and electron densities at  $0.85 \text{ V}$  applied bias leads to the observed quenching of PL in Figure 1b. Beyond  $0.85 \text{ V}$  applied bias, the total electric field across the device reduces further and eventually works to collect the trap states at the illumination side of the device, causing an additional increase of the electron-trap density overlap and quenching the PL lifetime as seen in Figure 1c. We note that one possible candidate for these charged trap states could be  $\text{MA}^+$  interstitials in the perovskite crystal, since these defects are positively charged, and have previously been observed in  $\text{MAPbI}_3$  to move on a similar timescale to the dynamics in Figure 1b.<sup>[37]</sup>

## 2.2. Dynamic Interaction of Trap States, Electric Fields, and Halide Segregation

It is important to understand how both the mobile trap states discussed above and electric fields will affect the halide segregation dynamics in a mixed-halide perovskite device, as this may provide insight into the underlying segregation mechanism. To study the dynamic ion segregation and remixing processes—as opposed to focusing on the equilibrium state reached by the segregating perovskite as was done in Figure 1—we repeatedly exposed a fresh mixed-halide perovskite device to 1 min intervals of illumination under  $110 \text{ mW cm}^{-2}$  ( $\approx 1 \text{ sun}$ ), 400 nm, continuous wave light, followed by 30 min of darkness. The intervals of darkness lasted 30 times longer than the illumination intervals to ensure enough time for the segregated ions to remix.<sup>[15]</sup> Under darkness no voltage was applied across the device, and under illumination the device was held at various constant biases to vary the total electric field across the perovskite layer. As shown in the top panel of Figure 2a, the

applied bias was ramped up and down between 0 and 1 V in 0.1 V increments between illumination intervals. The up-down voltage ramp was performed 4 times in order to examine the repeatability of the PL behavior and to observe any significant long-term changes in the segregation dynamics, of which none were found. As before, the PL spectra were taken every 3 s within the illumination intervals, and the mixed-halide and iodide-rich perovskite PL peaks were integrated over (from 640 to 690 nm and 720 to 770 nm, respectively) to give integrated PL intensities, which are plotted in the bottom and middle panels of Figure 2a, respectively.

The middle and bottom panels of Figure 2a show that the PL emitted from the perovskite device varied considerably throughout the 88 illumination intervals over the course of the experiment. During each illumination interval, the middle panel of Figure 2a shows that the PL signal from the iodide-rich perovskite regions increased from near zero, and the bottom panel of Figure 2a shows that the mixed perovskite PL signal decreased. These PL changes are well-reported in the literature

to be the result of photoexcited charge-carriers funneling from the mixed perovskite phase into the forming regions of iodide-rich perovskite as halide segregation takes place.<sup>[15,32]</sup> The variation in PL over the multiple illumination periods resulted from a combination of the movement of charged trap states as observed in Figure 1 and—to a lesser extent—the change in extracted current from the device. As shown in Figure 1b, the effect of current extraction on the emitted PL from the perovskite layer (the sharp peaks and troughs in PL intensity that occur upon a voltage change) is quickly overwhelmed by the effect of the mobile trap states (the slower, asymptotic behavior of the PL after a voltage change), suggesting that the radiative efficiency of the perovskite is more heavily dependent on the distribution of the mobile trap states than on the current extraction efficiency. We therefore primarily attribute the changes in the emitted PL that occurred over the course of each individual illumination interval to the effects of halide segregation, and the changes that occurred over multiple illumination intervals to the motion of the mobile charged trap states.

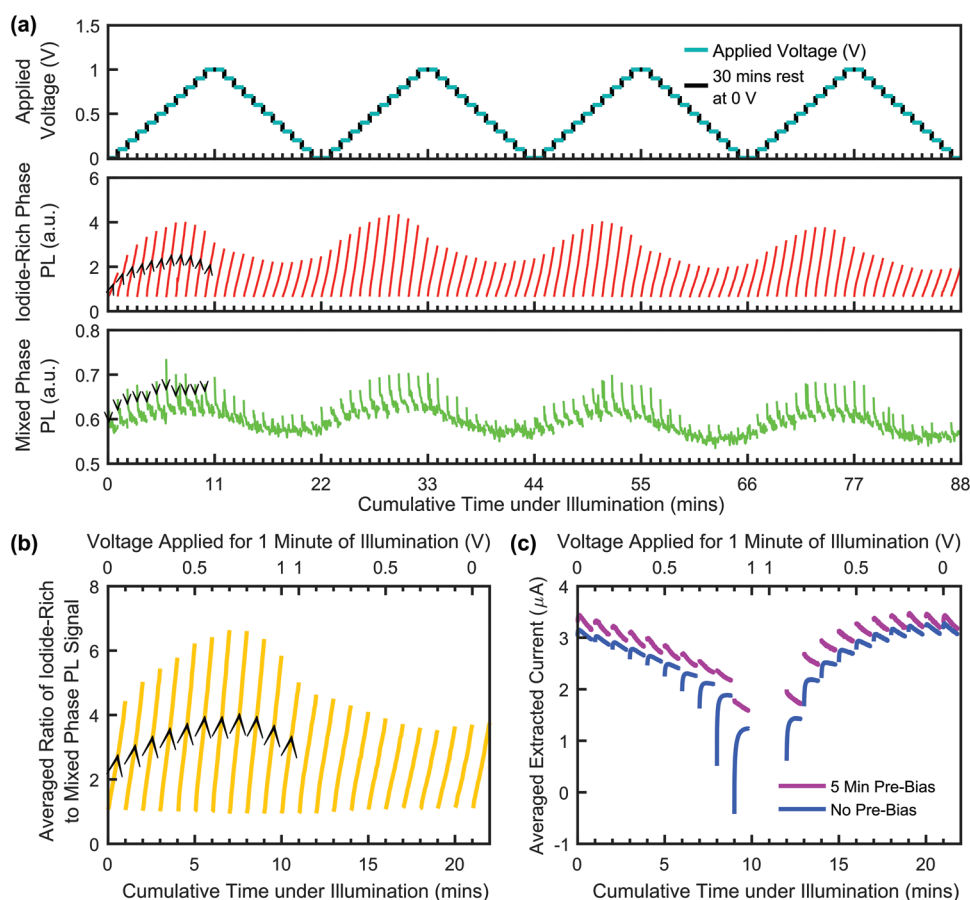


**Figure 2.** PL and extracted current measurements from a mixed-halide perovskite device as an applied voltage across the device is repeatedly ramped up and down between 0 and 1 V. a) Top panel: The voltages applied across the device and indication of the rest intervals during the experiment. Middle panel: The integrated low energy PL (720–770 nm) from the device under 400 nm, 110 mW cm<sup>-2</sup>, continuous wave illumination. Arrowheads over the first 11 illumination intervals help to indicate that, over the course of every illumination interval, the low energy PL increased in intensity due to halide segregation effects. Bottom panel: The integrated higher energy PL (640–690 nm) from the device. Arrowheads indicate that, over the course of every illumination interval, the higher energy PL decreased in intensity due to the effects of halide segregation. b) The ratio of the PL signals from the middle and bottom panels of (a), averaged across the last 3 voltage up-down ramps. Arrowheads indicate that, over the course of every illumination interval, the ratio of the PL signals increased due to halide segregation effects. c) Averaged behavior of the extracted current from devices with and without a 5 min prebiasing period before illumination at applied voltage.

Over multiple illumination intervals, the PL signal at a given point in each 1 min interval (for example, the first or last PL measurement) modulated up and down over the course of the experiment. We attribute this modulation of PL seen in the middle and bottom panels of Figure 2a to the movement of the mobile trap states toward and away from the illumination side of the perovskite layer according to the applied voltage across the device. Interestingly, this modulation of PL is not quite in phase with the applied voltage ramp, as the largest PL signals were observed when  $\approx 0.7$  V were applied across the device, 0.3 V before the peak of the applied voltage ramp at 1 V. Additionally, the PL emitted from the perovskite layer is seen in the middle and bottom panels of Figure 2a to not only depend on the applied voltage across the device, but also on whether the voltage is ramping up or ramping down, i.e., the PL emitted from the perovskite is not solely dependent on the immediate conditions, but also on the history of the applied electric fields. The dependence on the previous history of the experiment can be thought of as hysteresis in the PL measurements across the voltage up-down ramp. The observed hysteresis suggests that the mobile trap states lag behind the applied voltage, which is expected, given that Figure 1b shows the trap states take  $\approx 10$  min to reach equilibrium, an order of magnitude more than the 1 min illumination intervals used in the multiple voltage ramp experiment. Additionally, the observed hysteresis in the PL in the middle and bottom panels of Figure 2a suggests that 30 min under darkness at 0 V applied bias was insufficient to return the mobile trap states to equilibrium. If the trap states reached the same equilibrium between every illumination interval, there would be no way for previous measurements to affect future ones. There are many reports in the literature that ionic diffusion in perovskites is slower under darkness than in the presence of illumination,<sup>[15,38–40]</sup> so it is not unreasonable that the trap states were unable to return to their steady-state distribution in the dark. While 30 min under darkness was observed to be enough to remix the halide ions that had segregated under illumination, the dynamics, length scales, and ionic species involved in halide segregation<sup>[41–43]</sup> and the observed trap movement are not necessarily expected to be similar, and so different timescales for returning to equilibrium under darkness at 0 V applied bias is not inexplicable.

In order to somewhat disentangle the amount of halide segregation that occurred over the course of each illumination interval from the modulation of the PL intensity that resulted from the movement of the mobile trap states, we plot in Figure 2b the ratio of PL signals from the iodide-rich and the mixed-halide regions of perovskite over the course of an average voltage ramp. The ratio of the 2 PL signals was averaged over the last 3 voltage ramps for clarity, with the data from the first voltage ramp excluded from the average to eliminate the effect of the initial state of the device from the periodic trend seen. During halide segregation, the PL signal from the iodide-rich regions of perovskite grows relative to the PL signal from the mixed perovskite phase, and so the ratio of the PL signals in Figure 2b represents a measure of the amount of halide segregation in the perovskite layer. While we acknowledge that a simple ratio of the PL signals is not sufficient to completely cancel out any potential effects of the mobile trap states, Figure 2b represents a simple halide segregation measure that is adequate enough

for our analysis. The large variation in the relative growth of the iodide-rich perovskite PL peak in Figure 2b suggests that the amount of halide segregation that occurred in the perovskite material differed considerably across the different illumination intervals throughout the experiment. To highlight the difference in halide segregation rate across the experiment presented in Figure 2, Figure S10 and S11 in Section S5.3 of the Supporting Information present the initial and final PL spectra from particular 60 s illumination intervals. The measure of halide segregation plotted in Figure 2b shows the same hysteresis across the applied voltage ramps as is observed in the PL signals in the middle and bottom panels of Figure 2a, suggesting both are influenced by the mobile trap states that lag behind the voltage ramp. Given that the largest amount of halide segregation is observed in Figure 2b at  $\approx 0.7$  V applied bias on the voltage ramp-up—when the PL is brightest—we conclude that a lack of interaction between the trap state and the photoexcited charge-carrier densities—which causes high PL emission—correlates with increased amounts of halide segregation.

### 2.3. Screening of Electric Fields by Ion Movement

In order to observe how mobile trap states and halide segregation will affect mixed-halide perovskite solar cells under photovoltaic operation, we plot in blue in Figure 2c the extracted current from our device during the PL experiment discussed above. Due to the high periodicity of the current measurements over the multiple voltage ramps up and down, equivalent points in the last 3 voltage up-down ramps were averaged over to produce the blue plots in Figure 2c. The entirety of the current data from this experiment is plotted in Figure S9 (Supporting Information). Because the illumination spot size was different to the device pixel active area, it is difficult to completely accurately calculate the current density from the extracted current. However, for reference, given that the laser spot size used was  $\approx 2.1 \times 10^{-4}$  cm<sup>2</sup> we expect 3  $\mu$ A of extracted current to roughly correspond to a 14 mA cm<sup>-2</sup> current density.

For any given illumination interval, the averaged extracted current plotted in blue in Figure 2c begins with a rapid initial rise. This type of fast current change is indicative of the well-studied phenomenon of current–voltage ( $J$ – $V$ ) hysteresis observed in metal-halide perovskite devices, where it has been observed that a rapid change in the applied voltage across the device results in a slower response (over the course of seconds) from the extracted current.<sup>[44–47]</sup> While the combination of a number of factors, including interface effects, is thought to give rise to  $J$ – $V$  hysteresis, it has been proposed that a significant part of the mechanism is comprised of slow ionic redistribution upon a rapid change in the applied voltage across the perovskite device.<sup>[44,45]</sup> In response to an electric field, mobile ions in the perovskite material set up a screening potential that affects the charge-carrier extraction efficiency from the film and modulates the trap assisted recombination. A change in the external electric field across the device results in a relatively slower change in the screening potential and the extracted current from the device.<sup>[48–51]</sup> We note that while the consensus is forming that ionic motion plays an important role in  $J$ – $V$  hysteresis, there are several other possible explanations that

have been put forward.<sup>[44,45,47,52]</sup> In the case of our voltage ramp experiment, the applied voltage across the device was 0 V in the dark, before being quickly switched to various voltages upon illumination. This rapid change in applied voltage would lead to a slower change (over the course of seconds) in the screening potential within the perovskite layer, resulting in the initial rise in extracted current observed in the blue plots at the start of every illumination interval in Figure 2c. The blue plots in Figure 2c show that the change in screening potential within the perovskite layer happened on the order of tens of seconds, much faster than the tens of minutes observed in Figure 1b required for the migratory trap states to reach equilibrium, which suggests that the screening ions are a different species to the mobile trap states.

#### 2.4. Summary of Defect Types

It is worthwhile at this point to briefly summarize our findings and discussions about the defect species within the perovskite layer of our devices. The data presented so far in this study allows us to distinguish between three different defect species in the perovskite material, each with different properties. First, Figure 1 shows that the radiative efficiency of the perovskite depends on the electric field applied across the material, which is indicative of a species of charged, mobile trap state. These trap states were observed to reach their equilibrium distribution on the order of tens of minutes under illumination, but were essentially stationary under darkness (see the discussion surrounding Figure 2a). Furthermore, given that we observed the highest emitted PL intensity from the perovskite when the overall electric field was directed away from the illumination side of the device where the density of photoexcited charge-carriers is highest, we can conclude that this species of trap state is positively charged. We propose that these defects could be interstitial MA<sup>+</sup> ions in the perovskite crystal, which have previously been observed in MAPbI<sub>3</sub> films to migrate under an applied bias on similar timescales.<sup>[37]</sup>

Second, in our previous work we observed that the rate of halide segregation in MAPb(Br<sub>0.5</sub>I<sub>0.5</sub>)<sub>3</sub> thin films is positively correlated with the fraction of photoexcited charge-carriers that undergo trap-mediated recombination, and we therefore concluded that some trap states in the perovskite material play an essential role in the halide segregation mechanism.<sup>[23]</sup> We suggested in our previous work that photoexcited electrons would be captured by these segregation-responsible trap states, setting up an electric field that would instigate the movement of the halide ions in the perovskite crystal. The responsible trap states therefore are likely to have an intrinsic neutral charge, as a negative charge would produce a low capture cross-section for electrons, and a positive charge would be partly or entirely neutralized by a captured electron, resulting in smaller electric fields within the perovskite and therefore a lower driving force for halide segregation upon illumination. We suggest that these segregation-responsible trap states are comprised of crystal lattice distortions located near the grain boundaries in the perovskite material, congruous with the evidence in the literature that these regions are strongly correlated with halide segregation.<sup>[41–43]</sup>

The interaction of the photoexcited charge-carrier density with both of these two trap states then explains the halide segregation dynamics captured in Figure 2b. While the charged, mobile trap states take no direct part in triggering the actual segregation process, they capture a fraction of the photoexcited charge-carriers that depends on the applied voltage. This in turn reduces the number of charge-carriers that are trapped by the neutral defect states. Since these latter neutral defect states become charged upon charge-carrier capture, they generate the electric fields that induce the segregation of halide ions.<sup>[23]</sup> Therefore, the charged, mobile trap states (proposed to be MA<sup>+</sup> interstitials) may suppress halide segregation by reducing the number of charge-carriers captured in neutral defect states (proposed to be lattice distortions located at grain boundaries) that directly trigger halide segregation. Thus, we propose that by competing with both the radiative recombination pathways and the halide segregation mechanism, the charged, mobile trap states cause the observed correlation between the radiative efficiency of the perovskite layer and the relative growth of the iodide-phase perovskite PL peak observed in Figure 2b.

Finally, the blue lines in Figure 2c show that a third species of defect is responsible for the fast screening of the perovskite material upon a change in the applied voltage. The corresponding defect species must necessarily be charged to induce a screening effect, and they were observed to reach equilibrium on the order of seconds to tens of seconds depending on the magnitude of the change in applied voltage, suggesting a high mobility. We propose that these defect states are interstitial halide ions and/or halide ion vacancy sites in the perovskite crystal, which are calculated to have the highest mobility and lowest activation energy for transport out of the ionic species in several different MHPs,<sup>[53–55]</sup> and have gained support in the literature as the cause for *J*–*V* hysteresis in perovskite photovoltaic devices.<sup>[44]</sup>

### 3. Current Extraction Dynamics

As real-world solar cells are subjected to both solar illumination and applied voltages, it is important to understand how halide segregation and different biases affect the current extraction from mixed-halide perovskite photovoltaic devices. However, the dynamics of the extracted current plotted in blue in Figure 2c are affected by a complicated convolution of both halide segregation and ionic screening effects, making it difficult to determine the individual effects of each process. In order to observe the extracted current dynamics from a mixed-halide perovskite photovoltaic device without any short-time screening behavior, a similar voltage ramp experiment as discussed above was performed on a fresh device with a period of voltage pre-biasing across the device applied under darkness. The time under darkness was kept constant across the 2 experiments at 30 min, and for the prebias experiment the 30 min under darkness was broken up into 25 min at 0 V applied bias, and 5 min at the applied voltage of the next illumination interval. The current extracted from the device under illumination during the prebiasing experiment is plotted in purple in Figure 2c where, due to the high periodicity of the measurements, the extracted current at equivalent points in the last 3 up-down voltage

ramps are averaged together. The initial fast component of the extracted current dynamics visible in the blue plots is not visible in the purple plots in Figure 2c, suggesting that the prebias under darkness allowed the screening ions to redistribute before the illumination interval. In Figure S13 and S14 (Supporting Information) we explicitly show that during the 5 min prebiasing periods under darkness, the extracted current from the device changed as expected according to the variation in the screening potential. The removal of the initial fast component of the extracted current without any significant change to the behavior of the PL from the perovskite layer (shown in Figure S12 in the Supporting Information) further suggests that the screening ions and migratory trap states are different species. The fact that the extracted current from the prebiased device (purple plots in Figure 2c) was higher than the device that was not prebiased (blue plots in Figure 2c) even after the tens of seconds required for the ion redistribution is likely a result of device-to-device variations in the device batch. The PL emitted from the device during the prebiased experiment is shown in Figure S12 (Supporting Information), and is very similar to the PL shown in Figure 2a. A discussion of the slight differences in the PL from the prebiased and not prebiased experiments is also given in Section S6.3 in the Supporting Information.

Without the fast screening dynamic, the purple current extraction curves in Figure 2c better show the changes to the current resulting from halide segregation. During every illumination interval the purple curves in Figure 2c decrease, clearly indicating that halide segregation reduces the amount of current extracted from the device—as has been observed elsewhere.<sup>[17,18]</sup> As halide segregation takes place, the charge-carriers within the forming iodide-rich regions of perovskite experience a limited amount of spatial freedom, resulting in high charge-carrier densities and a high rate of radiative recombination.<sup>[15]</sup> Thus, the observed drop in current across the illumination intervals in Figure 2c was likely due to the rising rate of radiative recombination within the iodide-rich regions of perovskite competing against the charge-carrier extraction rate.

As demonstrated in Figure 2c and discussed above, halide segregation is detrimental for charge-carrier extraction from—and therefore potential device performance as reported in refs. [17–19]—mixed-halide perovskites. In order to gain a fuller understanding of the pathways experienced by charge-carriers in a segregated device, particularly as to whether funneled charge-carriers are completely constrained within the iodide-rich regions of perovskite or whether they can still be extracted, we performed EQE measurements on a fresh mixed-halide perovskite device as the perovskite segregated under illumination of an AM1.5 spectrum. The AM1.5 spectrum was generated by a class AAA Oriol Solar Simulator on an aperture size of  $0.0919\text{ cm}^{-2}$  at an integrated power of 0.6 suns ( $60\text{ mW cm}^{-2}$ ), and the device was held under vacuum at 0 V applied bias during the experiment. EQE spectra were taken every 4 s over the course of the 20 min of illumination, with the results plotted in Figure 3. Figure 3a displays the EQE spectra averaged over 196 s intervals, with an inset showing the extracted current density from the device over the 20 min of illumination. Figure 3b shows the fractional component of the

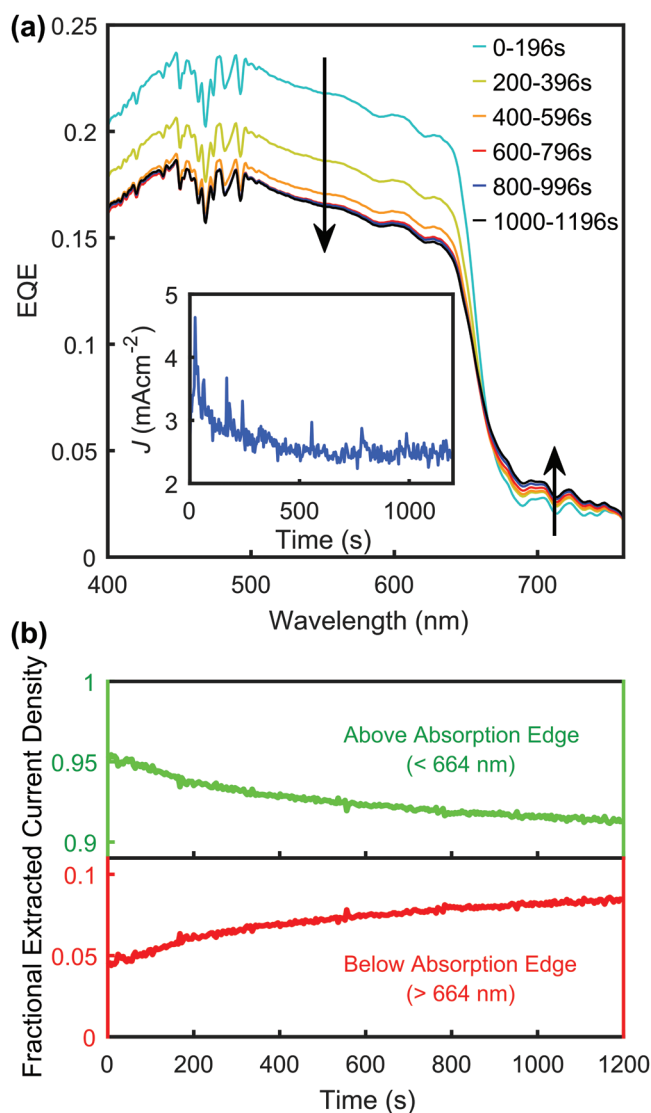


**Figure 3.** a) Evolution of the EQE spectra from a mixed-halide perovskite device under AM1.5 illumination at 0.6 suns ( $60\text{ mW cm}^{-2}$ ) for 20 min. Spectra were taken every 4 s and averaged over 196 s intervals. The extracted current density is plotted in the inset. b) Fractions of the extracted current density that originate from above (wavelengths shorter than 664 nm) and below (wavelengths longer than 664 nm) the absorption edge are plotted in green and red, respectively.

extracted current density attributed to the mixed (green) and iodide-rich (red) phases of the perovskite.

The EQE spectra display a sharp onset at 664 nm, which corresponds to the absorption edge of the fully mixed perovskite phase (Figure 3a). At longer wavelengths, below the absorption edge, the contribution to the EQE is attributed to the regions of iodide-rich perovskite that formed as the material segregated. Over time the EQE below the absorption edge (wavelengths longer than 664 nm) in Figure 3a increased, indicating that more light was absorbed and more current was extracted from the forming iodide-rich regions of perovskite as the perovskite segregated. Conversely, there is a dramatic loss in EQE above the absorption edge (wavelengths shorter than 664 nm) over

time, attributed to photoexcited charge-carriers generated within the mixed phase funneling into the iodide-rich regions of perovskite where the current extraction efficiency was lower. The inset of Figure 3a shows that as more charge-carriers funneled into these low extraction efficiency regions over time, the overall current density extracted from the device decreased. The decrease in this short circuit current is similar to previous reports of the detrimental nature of halide segregation on mixed-halide perovskite photovoltaic devices.<sup>[17–19]</sup>

Plotted in red in Figure 3b is the fractional contribution to the extracted current density from the iodide-rich regions of perovskite, which clearly increases as the halide segregation process occurs. Importantly, this contribution to the extracted current proves that charge-carriers can move from the low-bandgap regions of perovskite into the charge-carrier collection layers in the device. This extraction of charge-carriers from the low-bandgap regions happens despite the fact that the iodide-rich regions are known to comprise only a small fraction of the volume of the segregated perovskite layer,<sup>[15]</sup> and the energy required to escape these low-bandgap regions into the fully mixed perovskite phase ( $\approx 200$  meV) is greater than the thermal energy available to the charge-carriers at room temperature ( $\approx 30$  meV). In order to explain how the low-energy charge-carriers transferred into the extraction layers we note that the iodide-rich regions of perovskite are reported to preferentially form around the grain boundaries in the perovskite material.<sup>[41–43]</sup> While the effect of grain boundaries on charge-carrier lifetimes is still under debate,<sup>[24,25]</sup> charge-carrier transport along perovskite grain boundaries has previously been reported.<sup>[56–58]</sup> Thus we propose that the grain boundaries within the perovskite layer act as percolation pathways for the low-energy charge-carriers, acting as a traversable network between the nearby iodide-rich regions of perovskite and the charge-carrier extraction layers. The overall loss of current density extracted from the device (inset of Figure 3a) suggests that the transport of the low-energy charge-carriers was not as efficient as the transport through the mixed perovskite phase. The low extraction efficiency from the iodide-rich regions of perovskite may result from an increased radiative recombination rate in these regions, or enhanced trap-mediated recombination at the grain boundaries,<sup>[24,25]</sup> reducing the lifetimes of the excited charge-carriers, as well as more disordered pathways along grain boundaries compared to the bulk.

#### 4. Charge-Carrier Pathways in Mixed-Halide Perovskite Photovoltaic Devices

The work we have reported up to this point grants good insight into the energy states and pathways experienced by the photoexcited charge-carriers in a segregated perovskite device. We summarize our findings in **Figure 4**: a Sankey diagram that represents the possible pathways from photoabsorption (top of diagram) to recombination event (bottom of diagram) for excited charge-carriers. We stress that the diagram is only meant to give a qualitative insight into charge-carrier dynamics in a segregating perovskite material as the rate of the various recombination mechanisms will depend heavily on the illumination parameters, exact material properties of the device layers, the

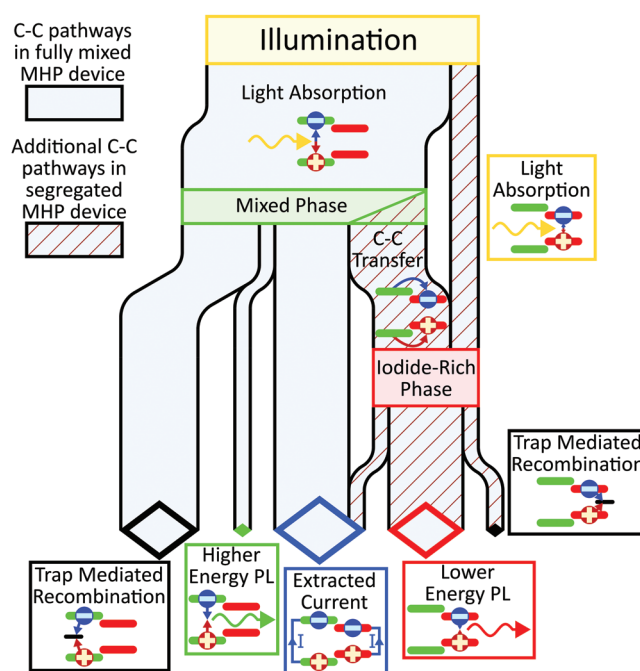


**Figure 4.** Sankey diagram representing the flow of photoexcited charge-carriers via various pathways in a fully mixed (solid pathways) and segregated (hatched and solid pathways) mixed-halide perovskite device. Every charge-carrier pathway begins with photoabsorption at the top of the diagram and finishes with a recombination event at the bottom (diamond boxes).

degree to which halide segregation has taken place, the applied voltage across the device, and the precise microstructure of the segregated domains. Auger recombination has been ignored as a higher order process that is negligible under typical real-world solar illumination intensities.<sup>[36]</sup> The mixed and iodide-rich perovskite phases are represented in the diagram as green and red boxes respectively, and recombination events are represented as diamond shaped boxes of various colors.

In a normal photovoltaic device, where the working layer is composed of one phase only, there are three main recombination pathways for the photoexcited charge-carriers: trap mediated recombination, radiative recombination, and extraction and recombination via an electrical circuit. In a mixed-halide perovskite device, as the perovskite layer segregates, further pathways open up as the charge-carriers are able to transfer between the different perovskite phases. The solid pathways depicted in Figure 4 highlight that initially, prior to any segregation, the perovskite layer in the device is composed of one phase (the mixed perovskite phase depicted by the green box) and so recombination occurs in this phase either through trap states, radiatively, or through current extraction. These three recombination pathways persist as the perovskite layer segregates, and the hatched pathways in Figure 4 show the additional pathways—involving the iodide-rich regions of perovskite—that open up as halide segregation occurs. The rise in EQE at long wavelengths shown in Figure 3a—and absorption measurements in the literature<sup>[31,59–62]</sup>—prove that a small but not insignificant number of charge-carriers are directly photogenerated in the iodide-rich regions of the perovskite, which is reflected

in Figure 4 as the corresponding pathway into the red iodide-rich phase box. Additionally, the drop in mixed perovskite PL signal intensity indicated in the bottom panel of Figure 2a is attributed to a flow of charge-carriers from the mixed perovskite phase into the lower-bandgap regions of perovskite, which is depicted as a pathway between the two phases in Figure 4. With regard to the recombination dynamics of the iodide-rich phase, Figure 3 shows that some current is extracted from the low-bandgap phase,<sup>[18,31]</sup> and the middle panel of Figure 2a highlights the strength of the radiative efficiency of this phase. Additionally, as discussed earlier, the changes in the PL intensity presented in Figure 1b allows us to deduce that a significant amount of trap-mediated recombination occurs within the iodide-rich regions of perovskite, and that the rate of this trap-mediated recombination depends on the electric field applied across the perovskite layer. Figure 4 incorporates these recombination pathways as flows out from the iodide-rich perovskite phase, resulting in a complicated final flow diagram from illumination through to recombination. Figure 4 represents a good summary of the findings reported in this study, and reflects our understanding of the charge-carrier dynamics within a mixed-halide perovskite device.

## 5. Conclusion

In this work we have studied the interaction between halide segregation, electronic trap states, and electric fields in mixed-halide perovskite photovoltaic devices. Our results suggest the existence of three distinct types of defects within the MAPb(Br<sub>0.5</sub>I<sub>0.5</sub>)<sub>3</sub> perovskite material, each with different properties and effects on the perovskite material. One species of defect, while essentially stationary under darkness, was observed under illumination to redistribute over the course of tens of minutes upon a change in the bias across the perovskite layer, implying that the defect is charged and mobile. Additionally, this defect species was observed to heavily reduce the radiative efficiency of the perovskite material. We propose that this defect species consists of MA<sup>+</sup> interstitials in the perovskite, given similar work in the literature on the movement of MA<sup>+</sup> ions in perovskite materials.<sup>[37]</sup> Second, following our previous work we suggest that a second species of defect state is responsible for halide segregation in mixed-halide perovskites.<sup>[23]</sup> We posit that these defect states cause the observed segregation of halide ions by capturing photogenerated charge-carriers and generating electric fields, and we argue that they must therefore be intrinsically charge neutral when empty. Crystal distortions concentrated at the grain boundaries in the perovskite layer are suggested as a candidate for these charge neutral defect states. Third, a charged, highly mobile defect was observed to screen the applied voltage across the perovskite layer by redistributing over the course of tens of seconds. Given mobility and activation energy calculations in the literature,<sup>[53–55]</sup> we suggest that these defects consist of halide vacancies and/or interstitials in the perovskite material. Additionally, EQE measurements showed that charge-carriers can be extracted from the low-bandgap, iodide-rich regions of segregated perovskite into the charge-carrier extraction layers of the device. We propose that the grain boundaries within the perovskite material—previously shown

to be capable of charge-carrier transport<sup>[56–58]</sup>—provide a percolation network for the low-energy, photoexcited charge-carriers to traverse. Finally, we summarized our findings and understanding of the charge-carrier pathways within a mixed-halide perovskite material through a qualitative Sankey diagram, which stresses the interconnectivity—and provides a convenient summary—of a multitude of the processes reported in mixed-halide perovskites. The findings reported here contribute to our understanding of the ionic and charge-carrier processes within mixed-halide perovskite materials, particularly the interaction of these processes with electric fields—an essential consideration for working photovoltaic devices.

## Supporting Information

Supporting Information is available from the Wiley Online Library or from the author.

## Acknowledgements

The authors gratefully acknowledge financial support from the Engineering and Physical Sciences Research Council (U.K.) (EPSRC). A.J.K. thanks University College Oxford for graduate scholarship support from the Oxford-Radcliffe endowment. L.M.H. thanks the Alexander-von-Humboldt Foundation for support.

## Conflict of Interest

The authors declare no conflict of interest.

## Keywords

electric fields, halide segregation, perovskites, photovoltaic devices, trap states

Received: October 23, 2019  
Revised: December 18, 2019  
Published online: January 30, 2020

- [1] H. J. Snaith, *Nat. Mater.* **2018**, *17*, 372.
- [2] A. K. Jena, A. Kulkarni, T. Miyasaka, *Chem. Rev.* **2019**, *119*, 3036.
- [3] K. A. Bush, A. F. Palmstrom, Z. J. Yu, M. Boccard, R. Cheacharoen, J. P. Mailoa, D. P. McMeekin, R. L. Z. Hoye, C. D. Bailie, T. Leijtens, I. M. Peters, M. C. Minichetti, N. Rolston, R. Prasanna, S. Sofia, D. Harwood, W. Ma, F. Moghadam, H. J. Snaith, T. Buonassisi, Z. C. Holman, S. F. Bent, M. D. McGehee, *Nat. Energy* **2017**, *2*, 17009.
- [4] T. Duong, Y. Wu, H. Shen, J. Peng, X. Fu, D. Jacobs, E.-C. Wang, T. C. Kho, K. C. Fong, M. Stocks, E. Franklin, A. Blakers, N. Zin, K. McIntosh, W. Li, Y.-B. Cheng, T. P. White, K. Weber, K. Catchpole, *Adv. Energy Mater.* **2017**, *7*, 1700228.
- [5] G. E. Eperon, T. Leijtens, K. A. Bush, R. Prasanna, T. Green, J. T.-W. Wang, D. P. McMeekin, G. Volonakis, R. L. Milot, R. May, A. Palmstrom, D. J. Slotcavage, R. A. Belisle, J. B. Patel, E. S. Parrott, R. J. Sutton, W. Ma, F. Moghadam, B. Conings, A. Babayigit, H.-G. Boyen, S. Bent, F. Giustino, L. M. Herz, M. B. Johnston, M. D. McGehee, H. J. Snaith, *Science* **2016**, *354*, 861.

- [6] A. Rajagopal, Z. Yang, S. B. Jo, I. L. Braly, P.-W. Liang, H. W. Hillhouse, A. K.-Y. Jen, *Adv. Mater.* **2017**, *29*, 1702140.
- [7] D. Forgács, L. Gil-Escrig, D. Pérez-Del-Rey, C. Mombllona, J. Werner, B. Niesen, C. Ballif, M. Sessolo, H. J. Bolink, *Adv. Energy Mater.* **2017**, *7*, 1602121.
- [8] J. Tong, Z. Song, D. H. Kim, X. Chen, C. Chen, A. F. Palmstrom, P. F. Ndione, M. O. Reese, S. P. Dunfield, O. G. Reid, J. Liu, F. Zhang, S. P. Harvey, Z. Li, S. T. Christensen, G. Teeter, D. Zhao, M. M. Al-Jassim, M. F. A. M. van Hest, M. C. Beard, S. E. Shaheen, J. J. Berry, Y. Yan, K. Zhu, *Science* **2019**, *364*, 475.
- [9] P. Loper, B. Niesen, S.-J. Moon, S. Martin de Nicolas, J. Holovsky, Z. Remes, M. Ledinsky, F.-J. Haug, J.-H. Yum, S. De Wolf, C. Ballif, *IEEE J. Photovoltaics* **2014**, *4*, 1545.
- [10] W. Shockley, H. J. Queisser, *J. Appl. Phys.* **1961**, *32*, 510.
- [11] J. H. Noh, S. H. Im, J. H. Heo, T. N. Mandal, S. Il Seok, *Nano Lett.* **2013**, *13*, 1764.
- [12] T. J. Jacobsson, J.-P. Correa-Baena, M. Pazoki, M. Saliba, K. Schenk, M. Grätzel, A. Hagfeldt, *Energy Environ. Sci.* **2016**, *9*, 1706.
- [13] D. P. McMeekin, G. Sadoughi, W. Rehman, G. E. Eperon, M. Saliba, M. T. Horantner, A. Haghighirad, N. Sakai, L. Korte, B. Rech, M. B. Johnston, L. M. Herz, H. J. Snaith, *Science* **2016**, *351*, 151.
- [14] R. E. Beal, D. J. Slotcavage, T. Leijtens, A. R. Bowring, R. A. Belisle, W. H. Nguyen, G. F. Burkhard, E. T. Hoke, M. D. McGehee, *J. Phys. Chem. Lett.* **2016**, *7*, 746.
- [15] E. T. Hoke, D. J. Slotcavage, E. R. Dohner, A. R. Bowring, H. I. Karunadasa, M. D. McGehee, *Chem. Sci.* **2015**, *6*, 613.
- [16] E. L. Unger, L. Kegelman, K. Suchan, D. Sörell, L. Korte, S. Albrecht, *J. Mater. Chem. A* **2017**, *5*, 11401.
- [17] I. L. Braly, R. J. Stoddard, A. Rajagopal, A. R. Uhl, J. K. Katahara, A. K.-Y. Jen, H. W. Hillhouse, *ACS Energy Lett.* **2017**, *2*, 1841.
- [18] G. F. Samu, C. Janáky, P. V. Kamat, *ACS Energy Lett.* **2017**, *2*, 1860.
- [19] T. Duong, H. K. Mulmudi, Y. Wu, X. Fu, H. Shen, J. Peng, N. Wu, H. T. Nguyen, D. Macdonald, M. Lockrey, T. P. White, K. Weber, K. Catchpole, *ACS Appl. Mater. Interfaces* **2017**, *9*, 26859.
- [20] M. Hu, C. Bi, Y. Yuan, Y. Bai, J. Huang, *Adv. Sci.* **2016**, *3*, 1500301.
- [21] W. Rehman, D. P. McMeekin, J. B. Patel, R. L. Milot, M. B. Johnston, H. J. Snaith, L. M. Herz, *Energy Environ. Sci.* **2017**, *10*, 361.
- [22] Y. Zhou, Y.-H. Jia, H.-H. Fang, M. A. Loi, F.-Y. Xie, L. Gong, M.-C. Qin, X.-H. Lu, C.-P. Wong, N. Zhao, *Adv. Funct. Mater.* **2018**, *28*, 1803130.
- [23] A. J. Knight, A. D. Wright, J. B. Patel, D. P. McMeekin, H. J. Snaith, M. B. Johnston, L. M. Herz, *ACS Energy Lett.* **2019**, *4*, 75.
- [24] J. M. Ball, A. Petrozza, *Nat. Energy* **2016**, *1*, 16149.
- [25] S. D. Stranks, *ACS Energy Lett.* **2017**, *2*, 1515.
- [26] S. T. Birkhold, J. T. Pecht, H. Liu, R. Giridharagopal, G. E. Eperon, L. Schmidt-Mende, X. Li, D. S. Ginger, *ACS Energy Lett.* **2018**, *3*, 1279.
- [27] D. L. Jacobs, M. A. Scarpulla, C. Wang, B. R. Bunes, L. Zang, *J. Phys. Chem. C* **2016**, *120*, 7893.
- [28] Y. Zhang, Y. Wang, Z.-Q. Xu, J. Liu, J. Song, Y. Xue, Z. Wang, J. Zheng, L. Jiang, C. Zheng, F. Huang, B. Sun, Y.-B. Cheng, Q. Bao, *ACS Nano* **2016**, *10*, 7031.
- [29] X. Deng, X. Wen, C. F. J. Lau, T. Young, J. Yun, M. A. Green, S. Huang, A. W. Y. Ho-Baillie, *J. Mater. Chem. C* **2016**, *4*, 9060.
- [30] N. J. Jeon, J. H. Noh, W. S. Yang, Y. C. Kim, S. Ryu, J. Seo, S. Il Seok, *Nature* **2015**, *517*, 476.
- [31] R. G. Balakrishna, S. M. Kobosko, P. V. Kamat, *ACS Energy Lett.* **2018**, *3*, 2267.
- [32] D. J. Slotcavage, H. I. Karunadasa, M. D. McGehee, *ACS Energy Lett.* **2016**, *1*, 1199.
- [33] R. Brenes, C. Eames, V. Bulović, M. S. Islam, S. D. Stranks, *Adv. Mater.* **2018**, *30*, 1706208.
- [34] S. G. Motti, M. Gandini, A. J. Barker, J. M. Ball, A. R. Srimath Kandada, A. Petrozza, *ACS Energy Lett.* **2016**, *1*, 726.
- [35] C. Li, A. Guerrero, Y. Zhong, A. Gräser, C. A. M. Luna, J. Köhler, J. Bisquert, R. Hildner, S. Huettner, *Small* **2017**, *13*, 1701711.
- [36] M. B. Johnston, L. M. Herz, *Acc. Chem. Res.* **2016**, *49*, 146.
- [37] Y. Yuan, J. Chae, Y. Shao, Q. Wang, Z. Xiao, A. Centrone, J. Huang, *Adv. Energy Mater.* **2015**, *5*, 1500615.
- [38] J. Xing, Q. Wang, Q. Dong, Y. Yuan, Y. Fang, J. Huang, *Phys. Chem. Chem. Phys.* **2016**, *18*, 30484.
- [39] Y.-C. Zhao, W.-K. Zhou, X. Zhou, K.-H. Liu, D.-P. Yu, Q. Zhao, *Light: Sci. Appl.* **2017**, *6*, e16243.
- [40] G. Y. Kim, A. Senocrate, T.-Y. Yang, G. Gregori, M. Grätzel, J. Maier, *Nat. Mater.* **2018**, *17*, 445.
- [41] C. G. Bischak, C. L. Hetherington, H. Wu, S. Aloni, D. F. Ogletree, D. T. Limmer, N. S. Ginsberg, *Nano Lett.* **2017**, *17*, 1028.
- [42] W. Li, M. U. Rothmann, A. Liu, Z. Wang, Y. Zhang, A. R. Pascoe, J. Lu, L. Jiang, Y. Chen, F. Huang, Y. Peng, Q. Bao, J. Etheridge, U. Bach, Y.-B. Cheng, *Adv. Energy Mater.* **2017**, *7*, 1700946.
- [43] X. Tang, M. van den Berg, E. Gu, A. Horneber, G. J. Matt, A. Osvet, A. J. Meixner, D. Zhang, C. J. Brabec, *Nano Lett.* **2018**, *18*, 2172.
- [44] C. Li, A. Guerrero, Y. Zhong, S. Huettner, *J. Phys.: Condens. Matter* **2017**, *29*, 193001.
- [45] D. H. Song, M. H. Jang, M. H. Lee, J. H. Heo, J. K. Park, S.-J. Sung, D.-H. Kim, K.-H. Hong, S. H. Im, *J. Phys. D: Appl. Phys.* **2016**, *49*, 473001.
- [46] H. J. Snaith, A. Abate, J. M. Ball, G. E. Eperon, T. Leijtens, N. K. Noel, S. D. Stranks, J. T.-W. Wang, K. Wojciechowski, W. Zhang, *J. Phys. Chem. Lett.* **2014**, *5*, 1511.
- [47] B. Chen, M. Yang, S. Priya, K. Zhu, *J. Phys. Chem. Lett.* **2016**, *7*, 905.
- [48] G. Richardson, S. E. J. O'Kane, R. G. Niemann, T. A. Peltola, J. M. Foster, P. J. Cameron, A. B. Walker, *Energy Environ. Sci.* **2016**, *9*, 1476.
- [49] Y. Zhang, M. Liu, G. E. Eperon, T. C. Leijtens, D. McMeekin, M. Saliba, W. Zhang, M. de Bastiani, A. Petrozza, L. M. Herz, M. B. Johnston, H. Lin, H. J. Snaith, *Mater. Horiz.* **2015**, *2*, 315.
- [50] T. Zhang, H. Chen, Y. Bai, S. Xiao, L. Zhu, C. Hu, Q. Xue, S. Yang, *Nano Energy* **2016**, *26*, 620.
- [51] S. Ravishankar, O. Almora, C. Echeverría-Arondo, E. Ghahremanirad, C. Aranda, A. Guerrero, F. Fabregat-Santiago, A. Zaban, G. Garcia-Belmonte, J. Bisquert, *J. Phys. Chem. Lett.* **2017**, *8*, 915.
- [52] J. B. Patel, J. Wong-Leung, S. Van Reenen, N. Sakai, J. T. W. Wang, E. S. Parrott, M. Liu, H. J. Snaith, L. M. Herz, M. B. Johnston, *Adv. Electron. Mater.* **2017**, *3*, 1600470.
- [53] C. Eames, J. M. Frost, P. R. F. Barnes, B. C. O'regan, A. Walsh, M. S. Islam, *Nat. Commun.* **2015**, *6*, 7497.
- [54] J. M. Azpiroz, E. Mosconi, J. Bisquert, F. De Angelis, *Energy Environ. Sci.* **2015**, *8*, 2118.
- [55] J. Haruyama, K. Sodeyama, L. Han, Y. Tateyama, *J. Am. Chem. Soc.* **2015**, *137*, 10048.
- [56] B. P. Nguyen, H. R. Jung, J. Kim, W. Jo, *Nanotechnology* **2019**, *30*, 314005.
- [57] J. S. Yun, A. Ho-Baillie, S. Huang, S. H. Woo, Y. Heo, J. Seidel, F. Huang, Y.-B. Cheng, M. A. Green, *J. Phys. Chem. Lett.* **2015**, *6*, 875.
- [58] J.-J. Li, J.-Y. Ma, Q.-Q. Ge, J.-S. Hu, D. Wang, L.-J. Wan, *ACS Appl. Mater. Interfaces* **2015**, *7*, 28518.
- [59] S. J. Yoon, S. Draguta, J. S. Manser, O. Sharia, W. F. Schneider, M. Kuno, P. V. Kamat, *ACS Energy Lett.* **2016**, *1*, 290.
- [60] S. Draguta, O. Sharia, S. J. Yoon, M. C. Brennan, Y. V. Morozov, J. S. Manser, P. V. Kamat, W. F. Schneider, M. Kuno, *Nat. Commun.* **2017**, *8*, 200.
- [61] A. J. Barker, A. Sadhanala, F. Deschler, M. Gandini, S. P. Senanayak, P. M. Pearce, E. Mosconi, A. J. Pearson, Y. Wu, A. R. Srimath Kandada, T. Leijtens, F. De Angelis, S. E. Dutton, A. Petrozza, R. H. Friend, *ACS Energy Lett.* **2017**, *2*, 1416.
- [62] W. Fan, Y. Shi, T. Shi, S. Chu, W. Chen, K. O. Ighodalo, J. Zhao, X. Li, Z. Xiao, *ACS Energy Lett.* **2019**, *4*, 2052.